Influence of Sodium Ions on the Dynamics and Structure of Single-Stranded DNA Oligomers: A Molecular Dynamics Study

José M. Martínez,[†] Sofi K. C. Elmroth,[‡] and Lars Kloo*,[†]

Contribution from the Department of Inorganic Chemistry, Royal Institute of Technology, Stockholm S-10044, Sweden, and Department of Inorganic Chemistry, Chemical Center, Lund University, P.O. Box 124, S-221 00, Lund, Sweden

Received April 4, 2001

Abstract: The effects of sodium counterion presence and chain length on the structure and dynamics of single DNA strands of polythymidylate were studied by means of molecular dynamics simulations. The importance of the base−base stacking phenomenon increases with the chain length and partially reduces the flexibility of the strand. Sodium ions directly interact with the phosphate groups and keto oxygens of the thymine bases, complexes showing lifetimes below 400 ps. Simultaneous phosphate and keto complexes were observed for one of the sodium ions with lifetimes around 1 ns. The implications of such complexes in the folding process experienced by the strand are considered. Structurally, cation inner- and outer-sphere complexes were observed in the coordination of phosphate groups. For the inner-sphere complexes, the structural information retrieved from the simulations is in very good agreement with experimental data. The diffusion properties of the sodium ions also reflect both types of coordination modes.

1. Introduction

The study of synthetic oligonucleotides has become a very active field due to their use as modulators of biological activity of DNA and RNA.[1] In many respects, the chemical properties of these oligonucleotides are likely to closely mimic the characteristics typical for their native counterparts. Examples include sequence-specific recognition by proteins[2] and (anticancer-active) metal complexes.[3] In contrast, the kinetic conditions for the approach of cations to small oligonucleotides has been shown to be substantially influenced even by small variations of the size of these fragments.[4−9] The mechanistic interpretation of such effects is currently hampered by the lack of relevant thermodynamic and dynamic data.

A fundamental feature of nucleic acid structure is the large degree of flexibility.[10] The different accessible conformations are dependent on enviromental factors such as solvent or counterions.[11,12] The interplay between structure and environment is a fundamental knowledge for the understanding of the function of these and other biomolecules. Structural and dynamical information can be obtained either experimentally,[11,13,14] mainly by X-ray crystallography and NMR spectroscopy, or theoretically,[13,15−17] by quantum chemical computations and molecular dynamics (MD) and Monte Carlo (MC) simulations. The dynamics of double-stranded DNA is reduced by the presence of hydrogen-bonding interactions between complementary bases in the antiparallel strands. The structure of single-stranded DNA, where such interactions are absent, can thus be expected to exhibit a much larger degree of flexibility. This observation highlights experimental difficulties because the information is obtained through data averages corresponding to different conformers. If a static view is applied, the data interpretation can lead to virtual structures. Among computational tools, statistical simulations are appropriate techniques for the analysis of the conformational properties of polynucleotides and for the description of interactions of noncovalent character, providing that a reliable force field is employed. In a series of previous reports,[18−23] Norberg and Nilsson, using MD simulations, have performed a detailed study of the stacking/unstacking process over a large number of monophosphate dinucleotides present in DNA and RNA. These authors have investigated the process on the basis of mean force potential calculations using the base−base distance as reaction coordinate. The methodology has even been applied to a single strand containing three bases, where two reaction coordinates were used.[24] Koča and co-workers have developed a conformational search algorithm[25] and combined it with MD-simulated

[†] Royal Institute of Technology.
[‡] Lund University.

(1) Romano, G.; Mitcheli, P.; Pacilo, C.; Giordano, A. *Stem Cells* **2000**, *18*, 19−39.
(2) Nadassy, K.; Wodak, S. J.; Janin, J. *Biochemistry* **1999**, *38*, 1999−2017.
(3) Guo, Z. J.; Sadler, P. J. *Adv. Inorg. Chem.* **2000**, *49*, 183−306.
(4) Elmroth, S. K. C.; Lippard, S. J. *J. Am. Chem. Soc.* **1994**, *116*, 3633−3634.
(5) Elmroth, S. K. C.; Lippard, S. J. *Inorg. Chem.* **1995**, *34*, 5234−5243.
(6) Ericson, A.; Arthur, C.; Coleman, R. S.; Elding, L. I.; Elmroth, S. K. C. *J. Chem. Soc., Dalton Trans.* **1998**, *12*, 1687−1692.
(7) Ericson, A.; McCary, J. L.; Coleman, R. S.; Elmroth, S. K. C. *J. Am. Chem. Soc.* **1998**, *120*, 12680−12681.
(8) Kjellstrom, J.; Elmroth, S. K. C. *Inorg. Chem.* **1999**, *38*, 6193−6199.
(9) Ericson, A.; Iljina, Y.; McCary, J. L.; Coleman, R. S.; Elmroth, S. K. C. *Inorg. Chim. Acta* **2000**, *1−2*, 56−63.
(10) Dickerson, R. E.; Drew, H. R.; Conner, B. N.; Wing, R. M.; Fratini, A. V.; Kopkea, M. L. *Science* **1982**, *216*, 475−485.
(11) Saenger, W. *Principles of Nucleic Acid Structure*; Springer-Verlag: New York, 1984.
(12) Sigel, A.; Sigel, H. *Metal Ions in Biological Systems*; Marcel Dekker: New York, 1996; Vol. 32.
(13) Leontis, N. B., Santalucia, J., Jr., Eds. *Molecular Modeling of Nucleic Acids*; ACS Symposium Series 682; American Chemical Society: Washington, DC, 1997.
(14) Gorenstein, D. *Chem. Rev.* **1994**, *94*, 1315−1338.
(15) McCammon, J. A.; Harvey, S. C. *Dynamics of proteins and nucleic acids*; Cambridge University Press: Cambridge, 1987.
(16) Rappé, A. K.; Casewit, C. J. *Molecular Mechanics Across Chemistry*; University Science Books: Sansalito, CA, 1997.
(17) Hobza, P.; Šponer, J. *Chem. Rev.* **1999**, *99*, 3247−3276.
(18) Norberg, J.; Nilsson, L. *Biophys. J.* **1994**, *67*, 812−824.
(19) Norberg, J.; Nilsson, L. *J. Phys. Chem.* **1995**, *99*, 13056−13058.
(20) Norberg, J.; Nilsson, L. *J. Am. Chem. Soc.* **1995**, *117*, 10832−10840.
(21) Norberg, J.; Nilsson, L. *Biophys. J.* **1995**, *69*, 2277−2285.
(22) Norberg, J.; Nilsson, L. *Biopolymers* **1996**, *39*, 765−768.
(23) Norberg, J.; Nilsson, L. *Biophys. J.* **1998**, *74*, 394−402.
(24) Norberg, J.; Nilsson, L. *J. Phys. Chem.* **1996**, *100*, 2550−2554.
(25) Fadrná, E.; Koca, J. *J. Biomol. Struct. Dyn.* **1996**, *14*, 137−152.

10.1021/ja0108786 CCC: $20.00
Published on Web 11/14/2001

annealing[26,27] in order to identify the most representative conformers of a series of di- and trinucleotides. Solvent was implicitly taken into account by means of a distance-dependent dielectric constant, screening the electrostatic interactions. Finally, Erie et al.[28] have used the MC methodology for generating conformations of short single-stranded DNA from arbitrary initial states. However, as the authors point out, solvent effects were not considered.

All these reports present a common feature: a lack of information regarding the possible effects of counterions. In some cases, these were included in the simulated system but not explicitly studied, and in others, they were not considered at all. In aqueous solution, the binding of DNA to small counterions such as Na^+ is complicated by its dynamic character with typical time scales in the order of picoseconds.[29−31] This fact makes the MD technique an appropriate tool for the description of the interaction, as has been shown in recent MD studies where the influence of Na^+ ions on the structure of DNA duplexes[32−35] and quadruplexes[36,37] was investigated.

Quantum mechanics has also been used to study the interaction of metal ions with "pieces" of nucleotide strands. Fernando et al.[38] have performed cluster calculations in which a Na^+ ion interacts with a phosphate unit by means of solvent-separated interactions in order to predict nucleotide ionization potentials. The interaction of a large set of ions, bare and hydrated, with nucleobases, Watson−Crick base pairs and reverse-Hoongsten ones, using different levels of computation have been performed by Šponer and co-workers.[39−43] The results show that cooperative effects that increase base pairing are always considerably more important when the metal ion is bonded to purine bases. The nonadditivity effects, as well, are noticeably reduced when going from inner- to outer-sphere (solvent-separated) metal ion coordination, revealing the importance of including the solvent effects to properly describe the interactions.

In this work, we have performed MD simulations of a series of thymidine oligonucleotides, $(pdT)_n$, but paying attention to ion−strand interaction and to the influence of counterions, Na^+ in this case, on the dynamics and structure of the strand. The role of the chain length on the flexibility of the strand is considered as well. Although the use of empirical pairwise additive interaction potentials is a known limitation when describing ion−strand complexes, the use of a soft monovalent cation such as sodium and a pyrimidine base, such as thymine, considerably reduces the potential effects of this inadequacy.

Figure 1. Helical structure proposed in ref 50 for poly(dT).

2. Methodology

Simulation Details. All molecular dynamics simulations were performed with the DL_POLY package[44] using the all-atom Cornell et al.[45,46] force field to describe DNA strands and counterions, and TIP3P[47] for modeling the aqueous solvent. It is worth pointing out that parameters characterizing the short-range interactions of the sodium ions are taken from the original work of Åqvist[48] (concerning ion hydration) and adapted[49] for use in the framework of the AMBER force field. Three single DNA strands, differing in length, were studied: $(pdT)_2$, $(pdT)_4$, and $(pdT)_8$. For each strand, two different MD simulations were done, one without counterions and one with Na^+ ions (two, four, and eight, respectively). Hereafter, simulations without metal ions will be denoted by $(pdT)_n$, and those with them by $(pdT)_nNa_n$. All initial structures were constructed on the basis of the polythymidylate model proposed in ref 50, which suggests a right-handed single helix with thymine bases pointing away from the helix axis and without base stacking (see Figure 1). Each strand was immersed into a pre-equilibrated periodic box of water molecules. Final dimensions of the periodic boxes were $25 \times 25 \times 25$ Å^3, $30 \times 25 \times 30$ Å^3, and 45×37

(26) Fadrná, E.; Koca, J. *J. Phys. Chem. B* **1997**, *101*, 7863−7868.
(27) Stefl, R.; Fadrná, E.; Koca, J. *J. Biomol. Struct. Dyn.* **1999**, *16*, 1087−1095.
(28) Erie, D. A.; Breslauer, K. J.; Olson, W. K. *Biopolymers* **1993**, *33*,-75−105.
(29) Bregadze, V. G. In *Metal Ions in Biological Sysytems*; Sigel, A., Sigel, H., Eds.; Marcel Dekker: New York, 1997; Vol. 32, Chapter 12.
(30) Guldbrand, L. E.; Forester, T. R.; Lynden-Bell, R. M. *Mol. Phys.* **1989**, *67*, 473.
(31) York, D. M.; Darden, T.; Deerfield, D.; Pedersen, L. G. *Int. J. Quantum Chem.: Quantum Biol. Symp.* **1992**, *19*, 145.
(32) Young, M. A.; Jayaram, B.; Beveridge, D. L. *J. Am. Chem. Soc.* **1997**, *119*, 59−69.
(33) Bonvin, A. M. J. J. *Eur. Biophys. J.* **2000**, *29*, 57−60.
(34) Hamelberg, D.; McFail-Isom, L. M.; Williams, L. D.; Wilson, W. D. *J. Am. Chem. Soc.* **2000**, *122*, 10513−10520.
(35) McConnelll, K. J.; Beveridge, D. L. *J. Mol. Biol.* **2000**, *304*, 803−820.
(36) Špačcková, N.; Berger, I.; Šponer, J. *J. Am. Chem. Soc.* **2001**, *123*, 3295−3307.
(37) Chowdhury, S.; Bansal, M. *J. Biomol. Struct. Dyn.* **2001**, *18*, 647−669.
(38) Fernando, H.; Kim, N. S.; Papadantonakis, G. A.; LeBreton, P. R. In *Molecular Modeling of Nucleic Acids*; Leontis, N. B., Santalucia, J., Jr., Eds.; ACS Symposium Series 682; ACS: American Chemical Society: Washington, DC, 1997; Chapter 2.
(39) Burda, J. V.; Šponer, J.; Hobza, P. *J. Phys. Chem.* **1996**, *100*, 7250−7255.
(40) Burda, J. V.; Šponer, J.; Leszczynski, J.; Hobza, P. *J. Phys. Chem. B* **1997**, *101*, 9670−9677.
(41) Šponer, J.; Burda, J. V.; Sabat, M.; Leszczynski, J.; Hobza, P. *J. Phys. Chem. A* **1998**, *102*, 5951−5957.
(42) Šponer, J.; Sabat, M.; Burda, J.; Sabat, M.; Leszczynski, J.; Hobza, P. *J. Phys. Chem. B* **1999**, *103*, 2528−2534.
(43) Gresh, N.; Šponer, J. *J. Phys. Chem. B* **1999**, *103*, 11415−11427.
(44) Forrester, T. W.; Smith, W. *DLPOLY* (2.1 version); CCLRC: Daresbury Laboratory, UK, 1995.
(45) Cornell, W. D.; Cieplak, P.; Bayly, C. I.; Gould, I. R.; Merz, K. M., Jr.; Ferguson, D. M.; Spellmeyer, D. C.; Fox, T.; Caldwell, J. W.; Kollman, P. A. *J. Am. Chem. Soc.* **1995**, *117*, 5179−5197.
(46) Force field parameters were taken from http://www.amber.ucsf.edu/amber/ff94/parm94.dat file.
(47) Jorgensend, W. L.; Chandresekhar, J.; Madura, J.; Impey, R. W.; Klein, M. L. *J. Chem. Phys.* **1983,** *79*, 926−937.
(48) Aqvist, J. *J. Phys. Chem.* **1990,** *94*, 8021.
(49) van der Waals parameters combining rules in ref 48 are different from those used in AMBER force field ($R^*_{ij} = R^*_i + R^*_j$, $\epsilon_{ij} = (\epsilon_i{}^*\epsilon_j)^{1/2}$). The adaption process consists, therefore, of finding the ϵ_{ion} and R^*_{ion} parameters using the AMBER combining rules and the TIP3P short-range parameters.
(50) Camerman, N.; Fawcett, J. K.; Camerman, A. *J. Mol. Biol.* **1976**, *107*, 601−621.

$\times$ 37 Å^3 for the dimer, tetramer, and octamer, respectively. Water molecules with an atom closer than 2.5 Å to any atom of the solute were removed, resulting in systems with 453, 665, and 1861 water molecules. For simulations including Na^+ ions, these were initially located along phosphate bisectors with a P−Na^+ distance of 6 Å. Prior to unrestrained MD, systems were relaxed by an energy minimization procedure: solvent molecules were initially relaxed, solute coordinates being fixed; the solute was then relaxed under fixed solvent coordinates; and finally solute and solvent molecules were relaxed together. After this energy minimization period, which covered several thousands of steepest-descendent steps, the systems were progressively heated to 300 K over 10 ps and equilibrated at this temperature for another 50 ps. After equilibration, a 1.25 ns production run was obtained for the dimer and tetramer simulations, while the two simulations containing the longest chain were extended up to 4.5 ns. The constant temperature algorithm of Nose-Hoover[51] with a coupling constant of 0.5 ps was used to control temperature. Bond lengths were fixed at their equilibrium values using the SHAKE[52] algorithm (tolerance 10^{-8}). The Verlet leapfrog scheme[53] was used for integration of equations of motions with a time step of 1 fs. A cutoff distance of 9 Å was used to evaluate Lennard-Jones interactions. Electrostatic forces were calculated by the Ewald sum procedure[53] with the same cutoff for the real-space part. The convergence parameter (α) and the largest reciprocal space vectors ($k_{max,i}$) were established[54] to obtain a relative error in the order of 10^{-6}. Simulations with net charged cells can be performed using an energy correction term that is physically equivalent to adding a uniform jelly of charge that exactly neutralizes the total cell charge.[55] Although more sophisticated corrections have been proposed,[56] these concern simulations in which the volume, the system shape, or the net charge is altered during the simulation process. None of those cases apply to the simulations presented here.

To check the known "flying ice-cube" effect,[57,58] the cell center of mass velocity, water diffusion, potential energy, and potential energy fluctuations have been checked during the simulations.[58] No evidence for that phenomenon was found in any of the cases, likely due to the high SHAKE tolerance imposed.

3. Results and Discussion

3.1. Strand Analysis. The root-mean-square deviations (RMSD) of snapshots from initial structures are shown in Figure 2. Initial fluctuations are large in magnitude; however, after 250−300 ps the long-term drift vanishes in all cases, and smaller fluctuations around steady values are observed. The average value of this parameter increases with chain length, the magnitude for simulations in the presence and in the absence of sodium counterions being similar. For the $(pdT)_8$ simulation, a very stable situation is found after 2.5 ns with an average RMSD value of 9.0 Å, while in the $(pdT)_8Na_8$ case that value is reached only in the last nanosecond of simulation.

The evolution of the structural parameters determining the backbone and sugar conformations and the sugar−base orientation during the course of the simulation has been done through the corresponding dials[59] (see Supporting Information). The probability distribution for each dihedral angle and sugar puckering (definitions in agreement with Saenger[11]), averaged over all nucleotides of a given chain, is collected in Figure 3. Information supplied by both representations is complementary: (i) the dials allow us to follow the temporary stability of the different conformations and can be used to connect transitions such as stacking/unstacking events with backbone parameters; (ii) the distributions will allow a clear definition of the regions preferentially sampled by the different parameters.

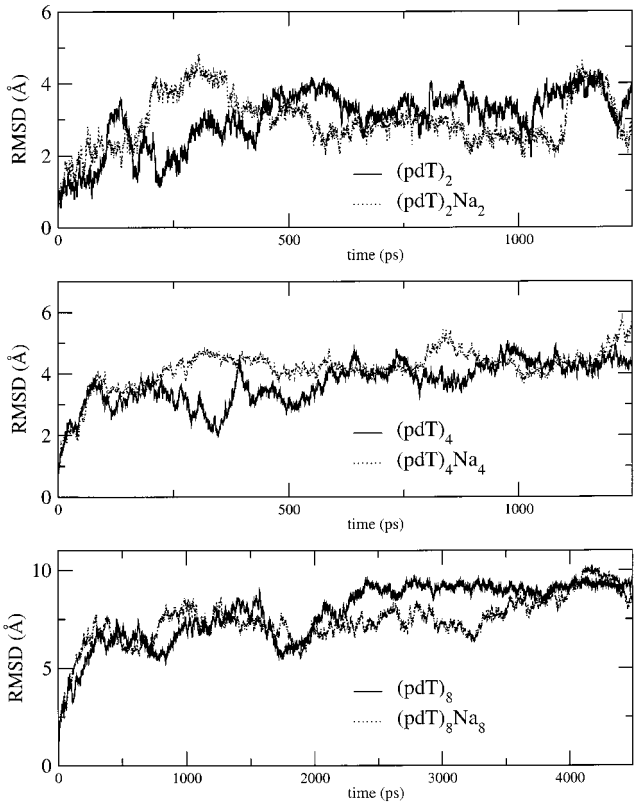

Figure 2. Root-mean-square deviation of oligonucleotide atoms from the initial structures as a function of time.

3.1.1. Dimer Simulations. The simulations (with and without sodium ions) show that the behaviors of the chains are quite similar, although some differences can be observed. Sugar puckering, described by the pseudorotation phase angle (P),[11] is preferred in the $C_{1'}$-exo/$C_{3'}$-exo region in both simulations. However, the structure of the furanose ring is rather flexible, showing frequent and nontemporarily stable excursions to the $C_{3'}$-endo region. This north ⇌ south conversion, most frequently found in the 3′-end nucleotide, is performed through the $O_{4'}$-endo intermediate state. The relative orientation of the thymine base versus the ribose ring, defined by the χ angle, is mainly anti (*-ac*), although in both cases the 3′-end nucleotide presents a larger flexibility in this parameter, and the syn region is sampled as well. Regarding backbone dynamics, only in a few cases is a defined orientation maintained during the whole simulation. This is the case for the β and δ dihedrals, which show single peak distributions around 180° and 135°, respectively. For the rest of the dihedrals involved in the backbone structure, a multipeak distribution is found, being quite similar for both simulations. Only slight differences in the relative population of the different clustering regions are found. This is particularly true for the α and ϵ dihedrals; although the *-sc* orientation is the most populated in both cases, the presence of Na^+ ions favor transitions to *+sc* and *-ap/-ac* orientations, respectively. However, one exception emerges from this pattern: the ζ angle. The simulation containing counterions shows

(51) Hoover, W. G. *Phys. Rev. A* **1985**, *31*, 1695.
(52) Ryckaert, J. P.; Ciccotti, G.; Berendsen, H. J. C. *J. Comput. Phys.* **1977**, *23*, 327.
(53) Allen, M. P.; Tildesley, D. J. *Computer Simulations of Liquids*; Clarendon Press: Oxford, 1989.
(54) Smith, W.; Forester, T. W. *The DL_POLY_2 User Manual* (Version 2.12); CCLRC: Daresbury Laboratory, UK, 1999; pp 93−95.
(55) Figueirido, F.; Del Buono, G. S.; Levy, R. M. *J. Chem. Phys.* **1995**, *103*, 6133−6142.
(56) Bogusz, S.; Cheatham, T. E., III; Brooks, B. R. *J. Chem. Phys.* **1998**, *108*, 7070−7084.
(57) Harvey, S. C.; Tan, R. K. Z.; Cheatham, T. E., III. *J. Comput. Chem.* **1998**, *19*, 726−740.
(58) Chiu, S-W.; Clark, M.; Subramaniam, S.; Jakobsson, E. *J. Comput. Chem.* **2000**, *21*, 121−131.
(59) Ravishanker, G.; Swaminathan, S.; Beveridge, D. L.; Lavery, R.; Sklenar, H. *J. Biomol. Struct. Dyn.* **1989**, *6*, 669−699.

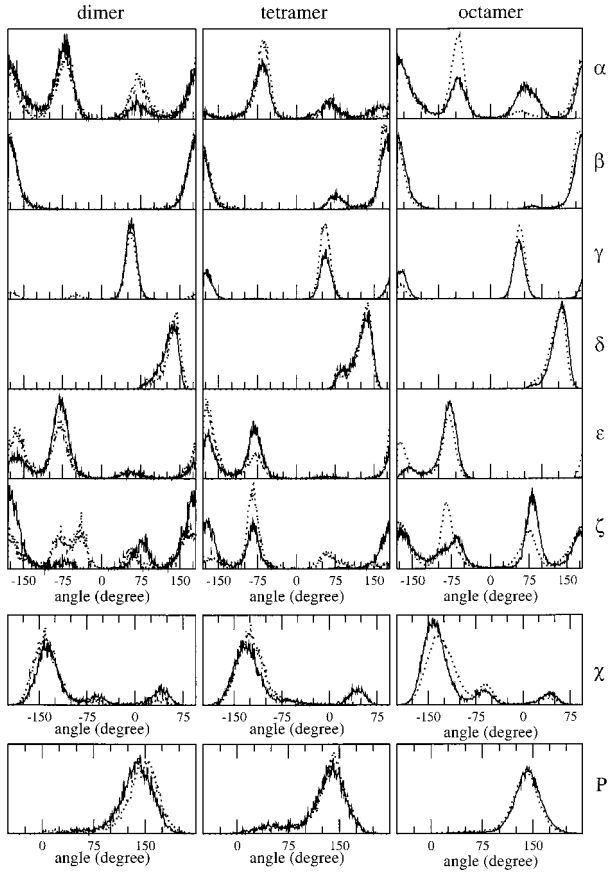

Figure 3. Backbone dihedral, sugar−base orientation and pseudorotation phase angle distributions for the $(pdT)_n$ (solid lines) and $(pdT)_nNa_n$ (dotted lines) simulations.

a different pattern for this parameter when compared to the one without them. In the case of the $(pdT)_2$ simulation, clustering in the $+sc$ and particularly in the *ap* region is observed. In the case of the $(pdT)_2Na_2$ system, despite showing a maximum of probability corresponding to the *ap* conformation, a shift to lower values for the maximum appearing in the $+sc$ is observed, and, especially, a large probability in the *-sc* region is displayed, in contrast to what is observed for the $(pdT)_2$ simulation.

The analysis of the dimer results is particularly interesting because the experimental information obtained from X-ray diffraction measurements is available.[50] Values are collected in Table 1, together with the mean values obtained from both dimer simulations. The agreement between simulations and experimental results is only partial. Several factors may contribute to this discrepancy. First, the experimental data obtained are a function of factors which are not considered in the calculations, i.e., crystal packing forces (intermolecular base−base stacking is present) and solvent-dependent structural conformations (crystals were obtained from a mixture of 50% ethanol in water). Second, applying a static view to the chain structure is difficult, as revealed by the large standard deviations obtained for some of the chain parameters. Despite all these considerations, both model and experiment propose an open structure without base−base intramolecular stacking. To stress this point, Figure 4 shows the evolution, along the simulations, of the distance between the two bases, using the N_1 atoms as references (R_{N1-N1}). This parameter is known (see for instance ref 19) to be highly correlated with the relative base−base orientation. Part b of the same figure shows the angle Θ defined by the two vectors perpendicular to the base plane. For distances equal or lower than ca. 5 Å, the orientation of bases becomes either parallel or antiparallel, i.e., Θ values close to 0° and 180°, respectively. The $(pdT)_2Na_2$ simulation clearly exhibits a larger tendency toward stacked conformations with $R_{N1-N1} \approx 5$ Å, corresponding to either parallel or antiparallel relative orientations. On average, and particularly for the simulation without sodium ions, these results bring out an image in which base−base stacking is not characteristic for the dimer.

3.1.2. Tetramer and Octamer Simulations. When going to longer strands, the appearance of base−base stacking phenomena reduces the flexibility and open character of the structure as compared with the dimer. The accessible range of parameter values for the backbone structure thus becomes more tightly defined. Although it is known that the stability of stacked aromatic rings is highly dependent on the dispersion forces, despite its simplicity, the AMBER force field is able to reproduce the main features of this phenomenon when comparisons with high-level (correlated) quantum chemical calculations are performed.[17] For longer chains, the information shown in Figure 4 can be more conveniently presented in terms of probabilities, because of the increasing number of consecutive base pairs. Figure 5 shows the histograms obtained for R_{N1-N1} and Θ parameters for all consecutive pairs present in the different chains. Two main conclusions from such plots can be extracted at two different levels. First, the base−base stacking becomes more important in the dynamics of the single DNA strands as the chain length increases: well-resolved peaks appear at distances lower than 5 Å and angles below 15°, for base−base distance and angle, respectively. Second, the presence of counterions clearly favors the stacking phenomenon. In addition, although some base−base stacking is present in the $(pdT)_4$ simulation, simulations containing the counterions present the maxima at a lower mean distance and Θ angle (4.1 Å and 12°, respectively), favoring closer contacts between bases and, consequently, stronger correlations in terms of base−base orientation. The time evolution of the stacked states shows a large stability. In all cases, once formed, these remain stable during the rest of the simulation (tetramer simulations) or for more than 3 ns (octamer with counterions). It is worth pointing out that if only the first 1.25 ns of the octamer simulations are analyzed, i.e., the simulation period of the smaller chains, the conclusions previously extracted in terms of the base−base distance and relative orientation probabilities are maintained.

It is interesting to recognize the backbone parameters clearly connected with the base stacking/unstacking process. Such information can be inferred from the analysis of the dials (Supporting Information), in conjunction with the time evolution of base−base distances. By means of transitions to specific values, some of the parameters defining the chain structure were found to be directly connected with the stacking phenomenon. This is the case for ε and ζ dihedral angles, for which transitions to *ap* (180°) and *-sc/-ac* (270°), respectively, are always observed. In addition, χ angles defining base−sugar orientation for both nucleotides must be in *-ac* orientation and the angle between vectors perpendicular to base planes close to 0°, i.e., bases parallelly oriented. Figure 6 gives an example of such a direct influence of these parameters on the base−base stacking phenomenon. The time evolution of ε and ζ dihedrals together with the base−base distance for one of the observed events in the $(pdT)_8Na_8$ simulation is shown in that figure. The concerted motion between backbone dihedrals is relatively rapid: the unstacking → stacking transition takes about 15−20 ps in all cases. In the case of $(pdT)_2Na_2$, values for ε and ζ parameters corresponding to the stacked situation are simultaneously obtained during the simulation; however, the system has enough

Table 1. Mean Values and Standard Deviations of Backbone Dihedrals, Sugar−Base Orientation, and Sugar Puckering for $(pdT)_2$ and $(pdT)_2Na_2$ Simulations[a]

	$(pdT)_2$		$(pdT)_2Na_2$		exptl	
	nucleotide 1	nucleotide 2	nucleotide 1	nucleotide 2	nucleotide 1	nucleotide 2
α	249 ± 64	197 ± 70	205 ± 92	226 ± 99	282	294
β	181 ± 23	182 ± 19	180 ± 18	180 ± 21	174	184
γ	56 ± 11	56 ± 11	56 ± 11	104 ± 85	44	42
δ	131 ± 15	123 ± 19	135 ± 13	129 ± 22	149	152
ϵ	254 ± 31		248 ± 39		255	
ζ	166 ± 54		255 ± 85		164	
χ	224 ± 20	293 ± 78	226 ± 23	238 ± 57	212	215
P	140 ± 24	129 ± 29	147 ± 20	136 ± 42	164	173

[a] Experimental values from ref 37 are included as well. See Supporting Information for angle definitions. Values in degrees.

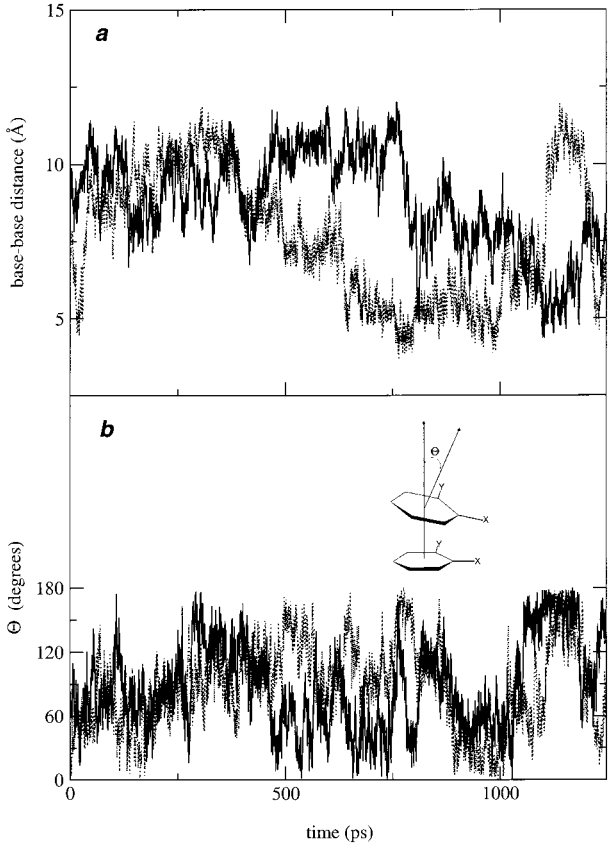

Figure 4. (a) N_1-N_1 distance as a function of time for the $(pdT)_2$ (continuous line) and $(pdT)_2Na_2$ (dotted line) simulations. (b) Relative base−base orientation.

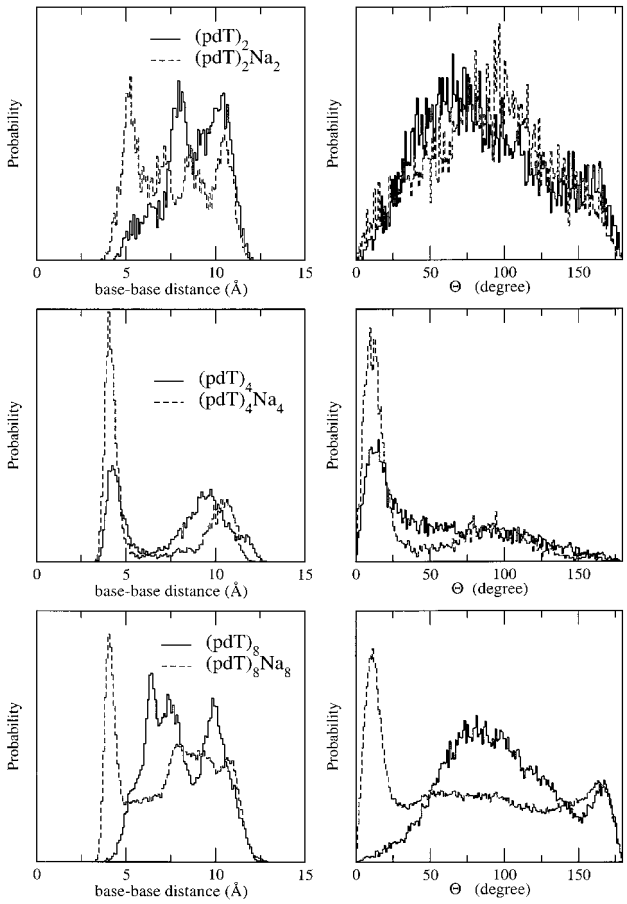

Figure 5. Probability distributions for the N_1-N_1 distance and base−base orientation.

freedom to leave it. Increasing the chain length limits the freedom of the backbone; once the stacked structure is formed it remains stable, provided that the above indicated values for *ϵ*, *ζ*, *χ*, and Θ angles are simultaneously obtained. Otherwise, fast base−base contacts are observed (R_{N1-N1} < 5.0 Å), but the situation is not stable and quickly evolves to an open type of structure. The stability of *properly* stacked bases has a clear influence on the dynamics of the stacking process: the next stacking event in the chain, if present, will involve one of the bases already stacked, producing two consecutive base pairs stacked. No preferential direction was observed for the third base to be stacked.

Stacking between nonconsecutive bases was also observed in the simulations containing the longest chain. In contrast to base−base stacking between consecutive bases, which occurred in the first 1.5 ns, nonconsecutive base stacking events are distributed along the whole simulation period (4.5 ns), involving bases belonging to units separated by one nucleotide or two nucleotides, i.e., nucleotides *i* and *i* + 2 or *i* and *i* + 3. In both cases, slider arrangements have been observed with a slightly longer base−base distance (4.5−5 Å). In the first case, the phosphate unit between the second and third nucleotides is kinked, bringing together the bases of the first and third units. These two bases become parallel because of the low-value syn region adopted by the *χ* parameter of the *i*th nucleotide, compared to the anti orientation adopted by the other two bases. The middle base remains rather far away from the other two bases (about 8 Å). In the second one, the backbone region belonging to both middle nucleotides is folded, allowing the two bases of the flanking nucleotides to become close enough to stack to each other. Interestingly, this phenomenon has been observed only once in each of the two longest simulations and in both cases involving bases belonging to nucleotides located in the middle region of the chain: nucleotides 4 and 7 and nucleotides 3 and 6 for the $(pdT)_8$ and $(pdT)_8Na_8$ simulations, respectively. In the first case, 2 ns of simulation was needed before the process was observed, while in the second case 3.5

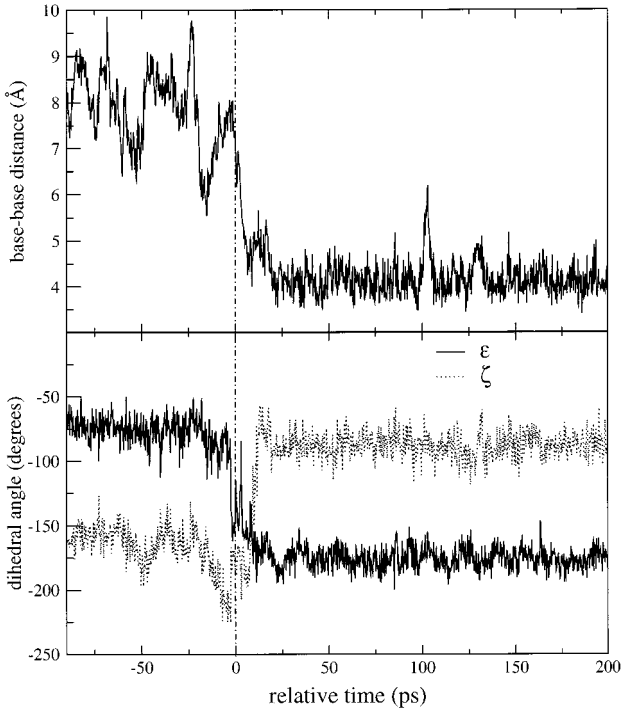

Figure 6. Evolution of the N_1-N_1 distance and ϵ and ζ backbone dihedrals during a unstacking → stacking event observed in the $(pdT)_8Na_8$ simulation.

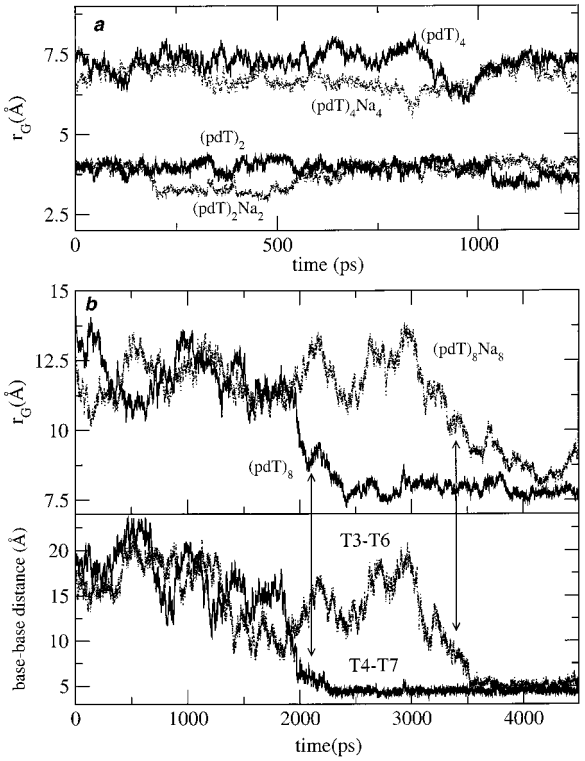

Figure 7. (a) Evolution of the radius of gyration (r_G) of the ssDNA molecules in the dimer and tetramer simulations. (b, upper) The same information as in part (a) but for the octamer simulations. (b, bottom) Evolution of the distances between bases T4 and T7 [$(pdT)_8$] and bases T3 and T6 [$(pdT)_8Na_8$].

ns was needed. In both cases, the stacked conformations remained stable during the rest of the simulations, having a great influence on the global shape of the strand. This fact can be observed by means of the time evolution of the radius of gyration (Figure 7), a magnitude that can also be used to check the effect of chain length on the backbone dynamics. The tetramer simulations are the ones showing a larger stacked-bases/number-of-nucleotides proportion, so the structure in these cases is more rigid, as can be seen from the standard deviations of the mean values for the radius of gyration (r_G). These are the same as those found in the dimer cases (∼0.3 Å), despite having twice the number of nucleotide units. In the case of the two octamer simulations, two different regions are found. In the first, with an average r_G value of 12.0 Å, large fluctuations are observed, mainly due to the freedom of the phosphate units located between nonstacked bases. These are able to adopt different and changing conformations, which is projected, for example, in the distance between the two terminal phosphate units: variations as large as 15 Å are present in both cases, showing structures with bending motions. In the second region, the structure adopted by the chain is more globular-like, and the average values of r_G are reduced to ∼8 and ∼9 Å for the $(pdT)_8$ and $(pdT)_8Na_8$ cases, respectively. The definition of these two regions is clearly correlated with the time evolution of the distance between the aforementioned bases (botton graph in Figure 7).

Despite these similarities, the average shapes corresponding to the second region identified in the radius of gyration graph are clearly different, as shown in Figure 8. In the absence of counterions, the strand adopts a more globular shape, while in the other case, the chain is folded in the central region, bringing together the two halves. The 3′-end half maintains its local stacked structure involving nucleotides 6, 7, and 8 for more than 2.5 ns, but when the folding process starts, the stacking between bases 7 and 8 is broken while the one involving nucleotides 3 and 6 becomes effective, the base of the nucleotide 3 interacting with that of nucleotide 5 as well. In this sense, the thymine group of nucleotide 3 is intercalated between those of nucleotides 5 and 6. The stability observed in the globular structure adopted by the chain of the $(pdT)_8$ simulation during the last 2.5 ns period can be understood on the basis of long-lived N—H···O hydrogen bonds, in some cases as long as 1.5 ns, between the NH groups of some thymine bases and the free oxygen atoms of phosphates or keto groups.

3.2. Counterion Analysis. The polydentate nature of nucleotides exhibited when interacting with metal ions is well known.[12] For alkali metal ions, the affinity for nucleotide-binding sites is rather nonspecific, and complexes with phosphate oxygens, ribose hydroxyls, and keto substituents are equally suitable.[11] The commonly accepted role of potassium and sodium ions is to serve as bulk electrolytes, to neutralize the negative charge of the polyanionic DNA strand. Due to the weakness of the complexes formed by the different biostructures (including proteins and membrane lipids) and alkali metal ions, binding sites for these are still poorly defined.[60] This is particularly obvious when compared with alkaline earth metal ions, especially Mg^{2+}.

The radial distribution functions (RDFs; obtained from statistical simulations) between Na^+ ions and different sites in the chain may supply primary information regarding ion−DNA interactions. The analysis of these functions revealed that only two main target places are found for sodium atoms: free (and negatively charged) phosphate oxygens and exocyclic thymine keto groups. However, no direct interactions were observed for other backbone or base groups. The corresponding RDFs for the three simulations containing counterions are plotted in Figure 9.

(60) Black, C. B.; Huang, H. W.; Cowan, J. A. *Coord. Chem. Rev.* **1994**, *135−136*, 165−202.

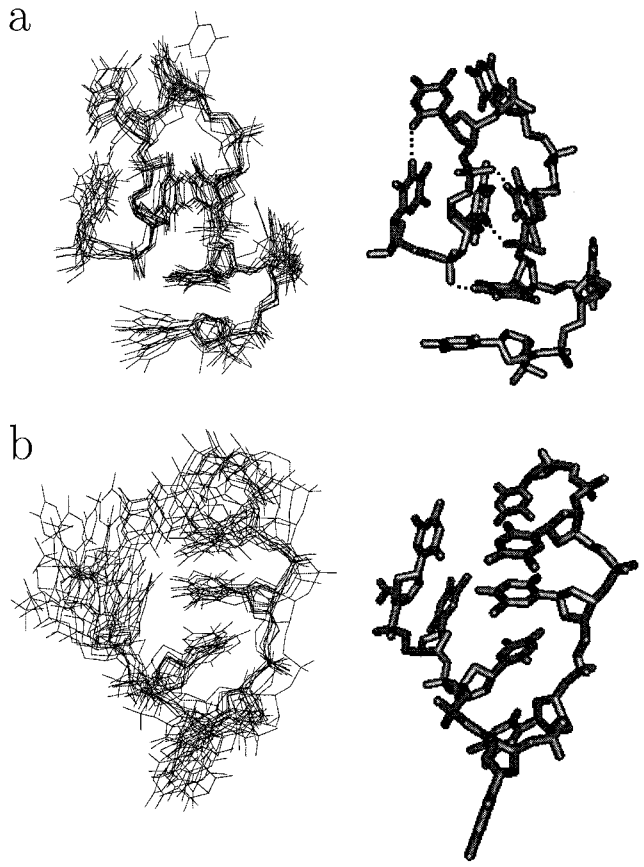

Figure 8. Calculated dynamical structure of the octamer based on 10 structures taken from the last half nanosecond in the $(pdT)_8$ (a) and $(pdT)_8Na_8$ (b) simulations. On the right side, average structures are shown, and for the $(pdT)_8$ case, long-lived hydrogen bonds are indicated.

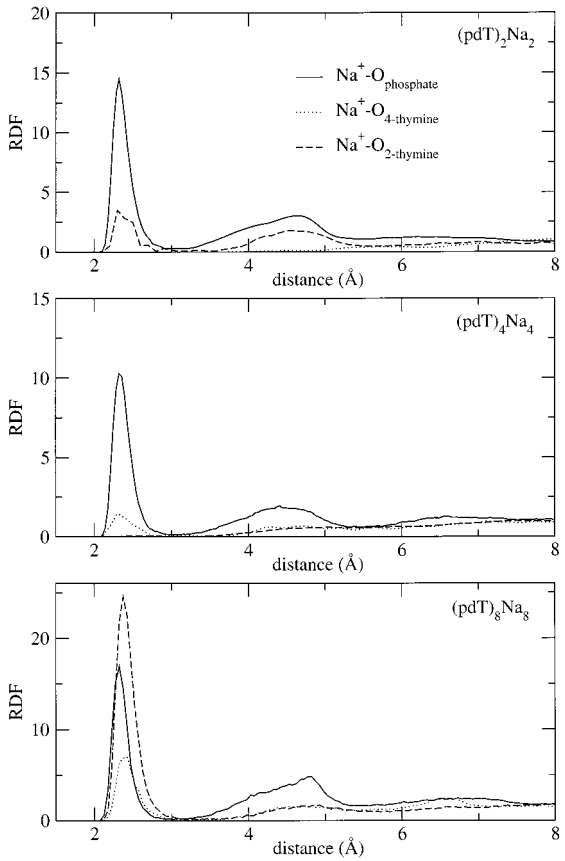

Figure 9. Radial distribution functions between sodium ions and oxygens of phosphate groups, and oxygens O4 and O2 of thymine bases.

Phosphate groups are clearly preferred by the counterions as compared to keto groups present in the nucleotide bases for the simulations containing the dimer and the tetramer, but not in the case of the longest chain. At first sight, the initial positions of the ions together with the shorter simulation periods of the smaller chains may indicate that, in these two simulations, no equilibration was reached for the ion distribution. Although this factor should certainly be kept in mind when comparing results among all three simulations, the preference observed in the RDFs for one of the keto groups in the $(pdT)_8Na_8$ simulation is the result of a very specific arrangement (addressed in section 3.2.3) involving one ion, and that accounts for half of the first peak observed in the corresponding RDF. Without that contribution, the distributions resulting for the $(pdT)_8Na_8$ simulation are highly similar to those of the shorter simulations and shorter chains, phosphate groups showing the highest probability as target sites of sodium ions.

3.2.1. Sodium−Phosphate Interactions. In all cases, $O_{phosphate}-Na^+$ RDFs show a sharp peak centered at 2.34 Å, and a less defined second region in the range 4−5 Å. The minimum between both regions is located at ca. 2.90 Å. The first peak corresponds to a direct inner-sphere binding of sodium ions to phosphates and the second to the interaction of the hydrated cation with the negatively charged backbone. This interpretation is based on the sodium−water RDF[48] that locates the maximum of the first coordination shell oxygen atoms at 2.40 Å and hydrogens at 3.05 Å. However, integration of these distributions up to the first minimum yields in all cases figures below 0.1 atom, meaning that under the conditions in which the simulations were performed, on average, the negatively charged part of the backbone is essentially only solvated by water. Two possible situations can be the cause: (i) direct metal−strand interactions are rare and have short mean lifetimes, or (ii) the distribution of counterions complexed by the strand is highly asymmetric. In the second situation, few and long-lived complexes are still possible, but when averaged along the strand they yield the distribution shown in Figure 9. The counterion distribution is indeed highly asymmetric, as shown by the radial distribution functions between Na^+ ions and the nonsterified oxygens of each phosphate group in the octanucleotide system (see Supporting Information).

The way Na^+ ions interact with the phosphate units can be rationalized on the basis of the coordination chemistry of this metal ion. Na^+ ion presents a hydration number of 5.8−5.9 (integration up to the first minimum in the $Na-O_{water}$ RDF) employing the interaction potentials used in our simulations. It reflects a dynamic picture of the hydrated ion in which five- and six-coordinated species are found, with a clear preference for the six-coordinated one. When the ion approaches the phosphate group, in which way is its nearest neighborhood altered? Figure 10a shows the evolution of the hydration number as a function of the P−Na distance. The hydration number coincides with the one found in the bulk down to ca. 4.4 Å, being reduced progressively for shorter distances and reaching a value around 4.0 for distances below 3.0 Å. This observed release of water molecules belonging to the first hydration shell of the metal ion is accompanied by the appearance of phosphate oxygens in the first coordination sphere of the ion (Figure 10b), which substitute for the leaving water molecules. Thus, the total coordination number becomes rather constant (Figure 10c) and almost independent of the relative positions of the ion and the phosphate units. These plots also show a continuous transition from a situation in which one phosphate oxygen is coordinating to a situation in which the two free phosphate oxygens are

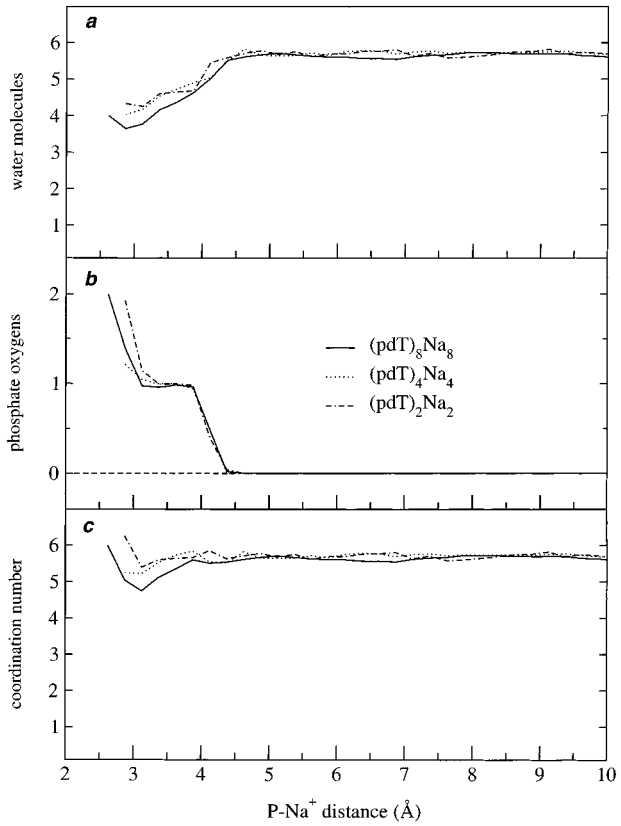

Figure 10. Number of water molecules (a) and phosphate oxygens (b) in the first coordination sphere of sodium ions as a function of the P−Na^+ distance. (c) Coordination number (sum of curves a and b).

coordinating the Na^+ ion (P−Na^+ distances in the 3−4 Å region and below 3 Å, respectively) as a result of the approach of the ion to the phosphate group. The image is better understood when some geometrical information is considered. Figure 11 shows the distribution (as a contour graph) of the angle (Φ) formed by the bisector of the O−P−O angle and the P−Na^+ vector obtained after projecting the Na^+ coordinates onto the O−P−O plane, as a function of the P−Na^+ distance. This graph is constructed on the basis of the information obtained from the three simulations containing counterions. In all cases, the pattern obtained is similar, differing only in the inherent statistics. This plot deserves several comments. First, there is a clear depletion zone of ca. 1 Å, which distinguishes the direct and solvent-separated ion−phosphate complexes, showing clearly the dual way in which ions interact with the phosphate units. In both situations the behavior is quite similar: shorter distances, closer to collinearity. For the shortest distances, the ion is located precisely along the line that bisects the O−P−O angle and, therefore, is equidistant from both oxygen atoms. However, this situation is by far the less representative from a probabilistic point of view. The distribution of the difference between the two O−Na distances for a given phosphate unit (not shown) indicates that the metal ion prefers an asymmetric coordination, in which it is coordinated to one oxygen, filling its first coordination shell with four or five water molecules. The graphic visualization of the representative structures provides, at least partially, an understanding of this result. Asymmetric metal−phosphate coordination allows the metal ion to interact with other phosphate groups or thymine bases, via solvent-separated complexes, or to interact directly with the O3′ or O5′ atoms of the same phosphate unit. Schneider and Kabeláč[61] have recently compiled the distributions of some metal ions around phosphate groups from crystal structures. Considering Na^+ positions closer than 3.0 Å to the charged phosphate oxygens, a wide ring-shaped coordination mode is found, in which the Na−O distance is constant, 2.4 Å, and the Na−O−P angle is about 125°. Using the same cutoff distance, our simulations yield 2.38 ± 0.14 Å and 135 ± 16° for the mean Na−O distance and Na−O−P angle. Taking into account the large standard deviation obtained for the second parameter, which certainly allows a large range of distributions, the agreement between both sources of information is quite high. In addition, Figure 11 shows a non-negligible population of Na^+ positions in which the ion is out of the sector O−P−O (values of cos Φ below ∼0.5). This fact is in agreement with the results of ref 61, where one of the two most probable binding sites for the sodium ion is found outside that sector, allowing the interaction with other groups in the chain. When the metal−phosphate interaction is mediated through water bridges, the situation changes slightly, and although an asymmetric distribution still is preferred, the symmetric disposition of the Na^+ ion with respect to the phosphate oxygens becomes more populated when compared to the direct ion−phosphate complexes.

The analysis of the conformation around phosphate groups during the periods when they complex a metal cation reveals the fact mentioned in the strand analysis section regarding the high probability experienced by the ζ dihedral angle of adopting an *-sc* conformation.

The mobility of the sodium ion is one of the properties that could be clearly affected by these interactions. Using the slope of the mean-square displacement (MSD) as the measure of the diffusion coefficient (*D*),

$$D = \lim_{t \to \infty} \frac{\langle [r(t) - r(0)]^2}{6t} \qquad (1)$$

three different situations have been identified, corresponding to different regions in the P−Na^+ RDF:

$$\text{I: } R_{\text{P}-\text{Na}^+} \leq 4.2 \text{ Å}$$

$$\text{II: } 4.2 \text{ Å} < R_{\text{P}-\text{Na}^+} \leq 6.5 \text{ Å}$$

$$\text{III: } 6.5 \text{ Å} < R_{\text{P}-\text{Na}^+}$$

Regions I and II correspond to the two types of complexes previously discussed, and region III can be associated with the "free" ions, i.e., those not complexed by the strand. For each ion, periods of at least 50 ps in the different regions were identified, and their diffusion coefficients were calculated using multiple time origins in eq 1 up to half of the period length, as previously done for the estimation of this magnitude in the case of second hydration shell water molecules of highly charged ions.[62,63] In this way, all the MSD points present equal statistics. Finally, the results were obtained by averaging the computed diffusion coefficients for each region. The value obtained for region III, $D_{\text{III}} = 2.40 \times 10^{-5}$ cm^2 s^{-1}, differs by 5% from the bulk value, 2.28×10^{-5} cm^2 s^{-1}, obtained for an aqueous solution[64] of Na^+ and, therefore, justifies the definition of the regions adopted. This bulk value overestimates by ca. 70% the

(61) Scheneider, B.; Kabeláč, M. *J. Am. Chem. Soc.* **1998**, *120*, 161−165.

(62) Martínez, J. M.; Pappalardo, R. R.; Sánchez Marcos, E.; Refson, K.; Díaz-Moreno, S.; Muñoz-Páez, A. *J. Phys. Chem. B* **1998**, *102*, 3272.

(63) Martínez, J. M.; Pappalardo, R. R.; Sánchez Marcos, E. *J. Chem. Phys.* **1998**, *109*, 1445.

(64) Simulation of one sodium ion in 400 TIP3P water molecules, using the same integration algorithm, time step, and temperature as those used in the simulations described in section 2.

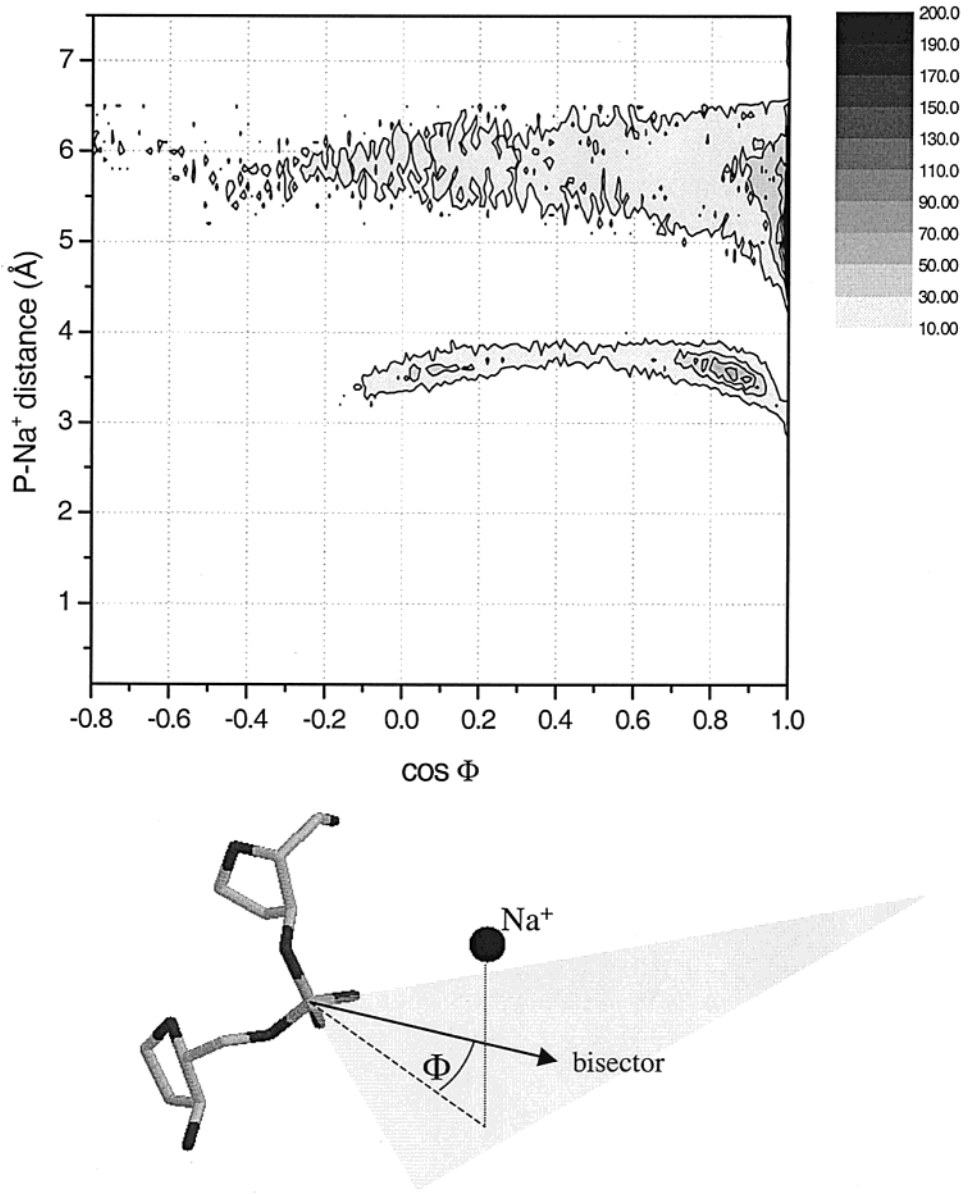

Figure 11. Distribution of sodium ions around phosphate groups: the probability distribution of cos ϕ as a function of the P−Na^+ distance. Definition of the ϕ angle is included in the bottom figure.

experimental value,[65] $D_{exp} = 1.33 \times 10^{-5}$ cm^2 s^{-1}. The large disagreement cannot be completely attributed to the ion−water potential: the water model used in our simulation, in conjunction with the use of the Ewald sum technique, overestimates by a similar percentage the solvent self-diffusion.[66] However, the relative values of the calculated different diffusion coefficients give information concerning how the complex formation influences the ion mobility. For regions I and II, a marked decrease is found with ratios $D_{II}/D_{III} = 0.48$ and $D_I/D_{III} = 0.28$, indicating how the mobility of the cation is limited by the interaction with the phosphate groups. These results are in agreement with the use of the three-site model[67] (free counterions, nonspecifically and specifically bound counterions) in the interpretation of quadrupolar NMR measurements[68] when studying ion binding in ordered systems such as macroscopically oriented DNA fibers.

3.2.2. Sodium−Base Interactions. In the case of the counterion−base interaction, RDFs plotted in Figure 9 show the first maximum for the keto oxygens centered at ca. 2.4 Å, again implying a direct ion−base interaction. A marked preference for the O2 atom is observed. The analysis of those periods in which the sodium ions directly interact with the keto oxygens yields a final hydration number of 4.8 for the Na^+ ion, which completes its coordination shell including the keto oxygen. Performing an analysis similar to that done for the phosphate case (configurations with O−Na^+ distances shorter than 3.0 Å), average values of 2.45 ± 0.15 Å and 152 ± 16° are found for Na−O distance and Na−O−C angle, respectively. In addition, sodium ions clearly prefer to be out of the base plane. This type of arrangement allows, in some cases, the simultaneous formation of solvent-separated complexes with phosphate groups. During these periods, two clear relative orientations of

(65) Lide, D., Ed. *CRC Handbook of Chemistry and Physics*; CRC: Boca Raton, FL, 1994.
(66) Feller, S. E.; Pastor, R. W.; Rojnuckarin, A.; Bogusz, S.; Brooks, B. R. *J. Phys. Chem.* **1996**, *100*, 17011−17020.
(67) Lindblom, G.; Lindman, B.; Tiddy, G. J. T. *J. Am. Chem. Soc.* **1978**, *100*, 2299−2303.
(68) Schultz, J.; Nordenskiöld, L.; Rupprecht, A. *Biopolymers* **1992**, *32*, 1631−1642.

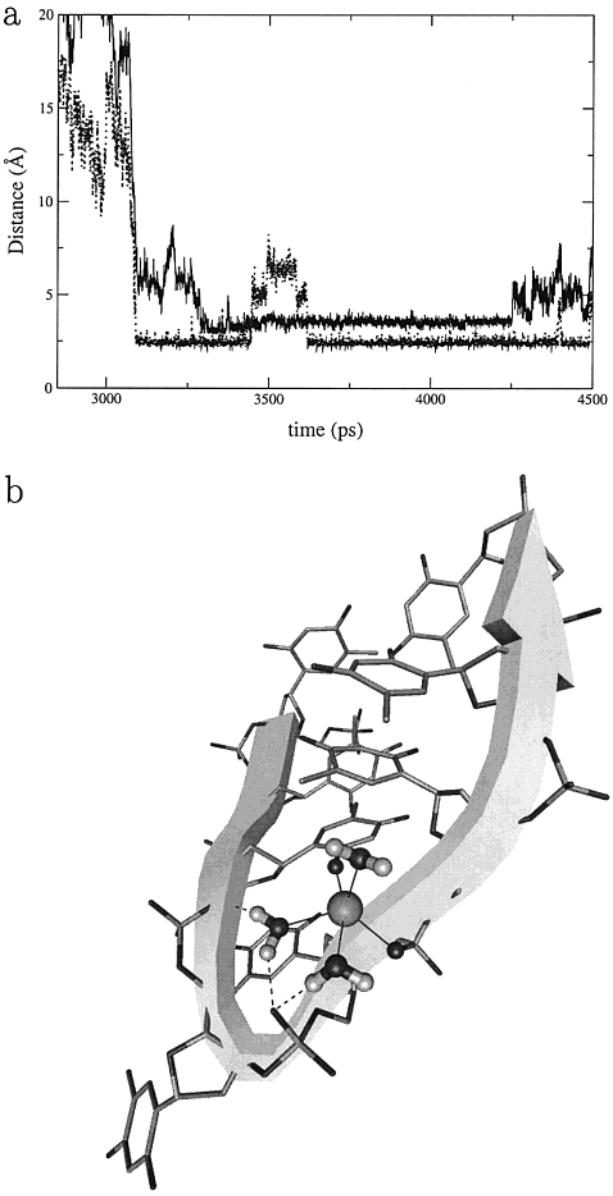

Figure 12. (a) Time evolution of the distances between Na^+ no. 2 and the phosphorus atom of the phosphate unit of nucleotide 6 (solid) and oxygen atom O2 of T3 (dashed). (b) Snapshot taken from the period shown in (a) displaying the coordination sphere (including water molecules) of the sodium ion. Hydrogen bonds involving solvent molecules are also shown.

the thymine base vs the ribose ring are found, clustering the values of the χ angle in both the anti (-*ac*) and syn (-*sc*) regions.

3.2.3. Simultaneous Metal−Phosphate and Metal−Keto Interactions: Influence on the Stability of the Folded Strand. The inner-sphere complexes previously discussed show in all cases lifetimes below 400 ps. However, the dispersion of values is considerable, ranging from 10−20 ps up to 350−360 ps. The highest stability is shown for the phosphate groups, with an average time of 177 ps, followed by the O2 keto oxygen, 153 ps, and finally by the O4 one with 66 ps. However, this picture does not apply once in the case of the $(pdT)_8Na_8$ simulation, in which substantially longer lifetimes are found for the inner-sphere complexes that involve one (O2) keto group and one phosphate unit, simultaneously coordinating the same sodium ion (no. 2). Figure 12a displays the time evolution of the distances between both groups and the metal ion, showing how the period in which these coordinating phenomena take place coincides with the folding process previously considered (Figure 7). The ion initially interacts with the keto group of nucleotide 3 and after ca. 200 ps becomes coordinated by one of the free oxygens of the phosphate group of nucleotide 6 as well. In this way, the metal ion is able to interact simultaneously with both halves of the chain and, particularly, in the region where the chain is bent. The first interaction is temporarily broken for about 170 ps and recovered again for almost 900 ps. The interaction with the phosphate groups is not broken and lasts for more than 1 ns. Although not shown in that figure, the ion is able to interact with yet a third group (phosphate unit of nucleotide 5) in the period 4150−4250 ps. During this whole period, the metal ion releases almost half of the water molecules of its hydration sphere, experiencing periods with only three water molecules in the first shell. Figure 12b shows one snapshot belonging to that period. Therefore, the stability previously found in the folded structure and attributed to the base−base stacking is now complemented by ion−strand interactions. The importance of monovalent metal ions as an integral part of RNA tetraloops has recently been shown by Basu et al.[69] by means of a potassium ion coordinated, as in our case, by several functional groups, including bases and phosphate units. The authors point out the likely participation of monovalent metal ions in the folding process.

Table 2. Mean Residence Times (ps) of Water Molecules in the First Hydration Shell of Sodium Ions in the $(pdT)_8Na_8$ Simulation[a]

Na^+ index	period (ns)	τ ($t^* = 0$ ps)	τ ($t^* = 2$ ps)
1,3−8	0−4.5	12.7 (0.5)	20 (1)
2	0−3.0	13.0	20
2	3−4.5	29.5	46

[a] Values in parentheses show the standard deviations obtained averaging results of all ions, except sodium no. 2.

This great stability found in the ion−chain interactions is also extended to the ion−water ones. In this sense, the probability of a given solvent molecule to remain in the hydration sphere of the ions has been computed. The so-called mean residence times (τ) have been computed using the method of Impey et al.[70] and are shown in Table 2. Within this model, the parameter t^* defines the maximum transient period a solvent molecule can leave the considered region, in this case the first hydration shell defined by the correponding ion−water RDF, without losing its ascription to it. Values of 0 ps[71] and 2 ps[70] have been frequently used in the literature and are applied in this work as well. Results obtained for Na^+ no. 2 in the first 3 ns of simulation perfectly fit the average behavior observed for the rest of the ions. However, when the period considered is the last 1.5 ns, the mean residence times computed for the water molecules around that ion become more than twice the average values, reflecting a situation in which the now partially hydrated ion presents a larger degree of inertness compared to the bulk situation.

4. Summary and Conclusions

The results presented in this work show how the increase of the nucleotide chain promotes the base−base stacking phenomenon, even in single-stranded nucleotides. In addition, the stacking/unstacking processes determine the rigidity of the nuecleotide strands, phosphate groups being the major pivots.

(69) Basu, S.; Rambo, R. P.; Strauss-Soukup, J.; Cate, J. H.; Ferré-D'amaré, A. R.; Strobel, S. A.; Doudna, J. A. *Nature Struct. Biol.* **1998**, *5*, 986−992.
(70) Impey, R. W.; Madden, P. A.; McDonald, I. R. *J. Phys. Chem.* **1983**, *87*, 5071.
(71) Garcia, A. E.; Stiller, L. *J. Comput. Chem.* **1993**, *14*, 1396.

This base−base stacking is favored in the simulations containing Na^+ ions mainly interacting with the phosphate units by means of monodentate complexes and to a large extent with one of the keto groups (O2) of thymine bases. In addition, the conformation of the phosphate groups is affected by the interaction with the metal ions, as revealed by the analysis of the ζ angle. Simulation times above 2 ns were necessary to observe folding processes for the octamer chains. The more globular-like structures were stabilized, in the absence of the counterions, by hydrogen bonding involving thymine bases and phosphate groups. In the presence of sodium ions, the bent structure is stabilized by stacking of nonconsecutive bases and ion−strand interactions in the bending region. These observations agree with the recent MD results of Špačcková et al.,[36] who found that the coordination of monovalent ions in four-thymidine loops of DNA quadruplexes competes with the formation of inter-thymine hydrogen bonds.

In general, lifetimes below the nanosecond region for direct sodium−DNA interactions are found, making the MD technique a useful tool for the study of complexes that have an active role in the structural and functional changes in biomolecules. Ion properties, such as mobility, are affected by the interaction with the strand. For the particular case of phosphate−sodium interactions, a model considering three different situations, i.e., free ion and outer- and inner-sphere complexes, seems to be adequate according to the mobility of the ion.

The observed base−base stacking interactions at room temperature in our simulations together with the possibility of bent or folded single DNA strands are in agreement with previous experimental findings. Vesnaver and Breslauer[72] point out the importance of recognizing some degree of order in single DNA strands when calculating the thermodynamic contribution of these to the duplex formation and how it is largely affected by the temperature. Even the possibility of initial single-stranded states forming hairpins is accepted as plausible. Our results seem to support that possibility as well. Furthermore, Garriga et al.,[73] studying cytosine homopolynucleotides, poly(dC) and poly(rC), present, in the case of the ssDNA, the absence of a monohelix structure but, at the same time, evidence for base−base interactions is found.

During the review of this manuscript, Sen and Nilsson[74] published a work in which MD simulations of single PNA, DNA, and RNA strands are presented. The authors investigate structural and dynamical features of homomorphous 10-mer strands with the explicit inclusion of water and sodium counterions, although these are not considered in the results analysis. The authors show how, in 1.5 ns simulations, there is a partial loss of the stacked arrangements used as initial setups. Shorter simulations (300 ps) are also performed for initially unstacked nonhelical conformations. Although the systems are different in nature and length, the comparison with our $(pdT)_8Na_8$ simulation is particularly interesting because in that work the CHARMM[75] force field was used and long-range electrostatics interactions were handled by a force-shifted cutoff methodology. In both cases the final structures contain stacked and unstacked segments, despite the completely different initial setups: totally unstacked or stacked situations. However, the authors do not describe any kind of globular or folding situations for their ssDNA simulations. At this point it is interesting to point out that the folding process in the $(pdT)_8Na_8$ simulation is observed after 3.5 ns, while the longest simulation period in their work is only 1.5 ns.

Finally, the Åqvist[48] potential parameters for Na^+, adapted to be used in the AMBER force field, have demonstrated their ability to reproduce the available structural information concerning the interaction of this ion with phosphate groups. These results support the use of such types of potential parameter combinations when soft metal ions must be included in biomolecular simulations. However, experimental information[61] should be used to check the ability of such strategies in the case in which ions with a higher charge are included, where the use of effective potentials becomes more complex due to the more relevant role of many-body effects in the nearest neighborhood of the ion. Efforts in that direction are ongoing in our laboratory.

Acknowledgment. The reviewers are acknowledged for their useful comments that have improved the manuscript. J.M.M. acknowledges financial support through the European Commission's Improving Human Potential Program Contract No. HPMF-CT-2000-00484 established by the European Commission. The Swedish Institute is also acknowledged for financial support, and NSC for the generous allocation of computing time.

Supporting Information Available: Dihedral angle definitions, dials, and phosphate−sodium radial distribution functions for the $(pdT)_8Na_8$ simulation (PDF). This material is available free of charge via the Internet at http://pubs.acs.org.

JA0108786

(72) Vesnaver, G.; Breslauer, K. J. *Proc. Natl. Acad. Sci. U.S.A.* **1991**, *88*, 3569−3573.

(73) Garriga, P.; Garcia-Quintana, D.; Manyosa, J. *Eur. J. Biochem.* **1992**, *210*, 205−210.

(74) Sen, S.; Nilsson, L. *J. Am. Chem. Soc.* **2001**, *123*, 7414−7422.

(75) Brooks, B. R.; Bruccoleri, R. E.; Olafson, B. D.; States, D. J.; Swaminathan, S.; Karplus, M. *J. Comput. Chem.* **1983**, *4*, 187−217.